sciendo Applied Mathematics and Nonlinear Sciences, 9(1) (2024) 1-15

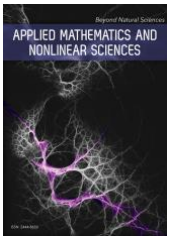

Applied Mathematics and Nonlinear Sciences

https://www.sciendo.com

Analysis of the effectiveness of virtual reality technology integration in landscape design

Fubin Li[1], Xia Zhao[1,†]

1. Academy of Fine Arts, Sichuan University of Science & Engineering, Zigong, Sichuan, 643000, China.

Submission Info

Communicated by Z. Sabir
Received January 6, 2023
Accepted June 23, 2023
Available online December 13, 2023

Abstract

In this paper, we first studied the 3D visual immersion technology of virtual reality, explored the stereoscopic display and multi-channel stereoscopic display method of virtual reality, and corrected the nonlinear distortion by grating alignment and deformation correction. After that, the model's lighting technology is examined, and the model's lighting coefficient is analyzed and calculated. Then, the advantages of landscape design based on virtual reality technology in terms of subjective evaluation, human perception, and promotion of work efficiency were analyzed by comparing traditional landscape design with virtual reality landscape design. The results show that the Sig value of the environmental adaptability of the two spatial designs is 0.037, which is less than 0.05, and there is a significant difference between the two in terms of subjective ratings. People's attention was enhanced by 7%-10% in the virtual design scene, and the induced brain frequency was 8%-10% higher than that of the traditional landscape design, indicating that the virtual landscape design was more effective.

Keywords: Virtual reality technology; Stereoscopic display; Lighting coefficient; Raster alignment; Landscape design
AMS 2010 codes: 97M50

†Corresponding author.
Email address: 1065285759@qq.com

ISSN 2444-8656
https://doi.org/10.2478/amns.2023.2.01471

1 Introduction

The development of digital technology plays a role in architectural landscape design brought about by each change, affecting the user's cognition and understanding of the way the design program, artificial intelligence and other high-speed development of science and technology so that the application of virtual reality technology in the interior design program began to emerge [1-2]. In the context of the experience economy, the value of commercial building interior space sensory experience and thinking identity gradually highlighted, and synergistic diversified industry has become an important demand of the current user consumption behavior [3-4].

The emergence of virtual reality, undoubtedly also for the innovative combination of art and technology in the field of architectural design to open up a new way of thinking, breaks the previous architectural design "from the plane, elevation, section and three-dimensional model" of the performance mode, the designer can at any time "into the" their own design scene space, from any angle to observe and review their design, immersive experience of space, scale, environmental light and even sound changes, so that the design of the Designers can at any time "into" their own design scene space, from any point of view to observe and review their design, immersive feel the space, scale, environmental light and even sound changes, so as to make the design creation more perfect [5]. The use of virtual reality for virtual indoor roaming so as to realize the evaluation of the interior design effect is a new attempt. Its purpose is in the planning and design stage so that people can be in a virtual three-dimensional environment, with a dynamic and interactive way to the future of residential immersive, all-round review [6-7].

Zhang, Y. et al. studied the cloud-based virtual reality voice landscape quantitative simulation design and analyzed the application of this voice landscape quantitative simulation design in outdoor design [8]. Zhang, X. et al. studied the virtual reality design method of interactive garden landscape and established a virtual environment with the ancient city of Yangcheng as the background [9]. Shi, G. et al. studied the multi-sensor information fusion technology based on a wireless virtual reality environment and discussed the implementation of a multi-sensor information fusion algorithm in intelligent art design [10]. Cai, K. proposes a new design method based on VR technology for environmental art design, which improves the problems in traditional environmental design [11]. Liao, J. Y. et al. studied the experience of the elderly in the use of immersive three-dimensional virtual reality and analyzed the acceptance of virtual reality technology by the elderly group [12]. Kong Y. et al. proposed a new method using virtual reality technology to study the interaction between humans and the built environment and analyzed the effectiveness of the method [13].

Zhou, Q. et al. studied the role of virtual reality technology in coastal urban design and explored the new thinking of architectural space design [14]. Ling, H. et al. studied the use of virtual reality in 3D terrain design and recustomized and developed the 3D terrain simulation system using Visual Basic 6.0 [15]. Lu, G. et al. elaborated the three-dimensional modeling method of virtual reality and constructed a new three-dimensional interactive virtual scene design method based on Unity 3D technology [16]. Dong, X. et al. studied the artistic style transformation based on 5G VR and VR visual space and analyzed the possibility and inevitability of VR technology and VR visual integration [17]. Wang, H. et al. studied the coastal landscape design method based on virtual reality technology and intelligent algorithm and discussed the advantages of virtual reality technology in landscape design [18]. Basu, T. et al. studied the principles and methods of visual design based on virtual reality, proposed a visual design creation system framework for intelligent human-computer collaboration, and applied virtual reality technology to architectural design [19]. Jing, W. et al. have studied the profound impact of virtual reality on environmental design, highlighting the value of virtual reality design in environmental design [20]. Kim, S. et al. studied urban design schemes assisted by

immersive virtual reality and explored the elements that affect the perception of urban quality of life [21].

This paper firstly explores the three-dimensional visual immersion technology of virtual reality technology, analyzes the principle and realization method of virtual reality technology in landscape design stereoscopic display generation, and further studies the method of multi-projection surface immersive virtual environment, non-linear distortion correction of multi-channel ring screen display system, fusion and seamless splicing of digital image edges of the screen, synchronization of data and inter-channel color and brightness balance, to realize the virtual reality landscape design three-dimensional display, so that users experience immersive landscape design immersion. Finally, the effect of virtual reality technology on landscape design is analyzed through the comparison of traditional and virtual scene design in subjective scores, EEG signals, and attention levels of different scenes to verify that the landscape design effect of virtual reality technology is more effective than the traditional according to the design effect.

2 3D visual immersion techniques for landscape virtual design

2.1 Landscape three-dimensional display

Realize the red and green stereo display first to generate red and green stereo image pairs, followed by an analysis of the red and green stereo image generation principle. As per research, the human brain is capable of receiving depth cues from the following four aspects. Depth cues in static images, depth cues caused by motion, physiological depth cues, and binocular parallax cues are studied here [22-23]. Figure 1 illustrates the binocular parallax. When looking at the same scene with both eyes, due to the different positions of the left and right eyes in space, the viewing angles of the two eyes will be different, the images seen will be different, and there will be parallax. The brain fuses the parallax images of both eyes to create a stereo image that contains stereo-depth information. A stereo image pair is a pair of two-dimensional images that have parallax visible to both eyes. If this pair of flat images is imitated and technical measures are taken so that the left eye can only see the image on the right and the right eye can only see the image on the left, then the human visual system will fuse a pair of slightly different images in the three-dimensional space, thus generating an image with stereoscopic perception. According to the projection surface, the human eye and the relative position between the observation object, there can be positive parallax (Figure b), negative parallax (Figure c) and zero parallax (Figure d).

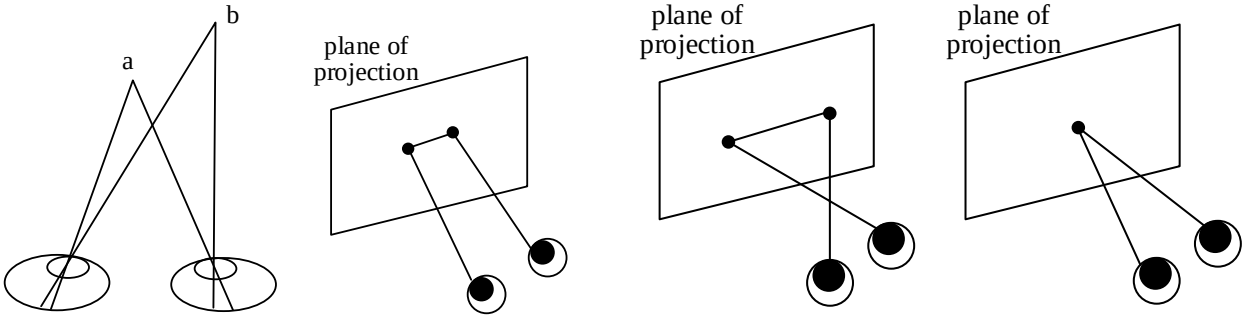

(a) binocular parallax image (b) ortho-parallax map (c) negative parallax map (d) zero parallax map

Figure 1. Vision difference

From the above study, it can be seen that stereo-image pairs are generated due to the different results of the perspective of the object observed by the left and right eyes. Therefore, two virtual eyes are set

up in the view simulation of stereoscopic display; one acquires the image of the left eye, and the other acquires the image of the right eye and transmits the images of the left and right eyes to the corresponding eyes, respectively. In the stereoscopic display, it is necessary to use a perspective projection method that includes two viewpoints and a double-center projection algorithm. Figure 2 shows the double center projection.

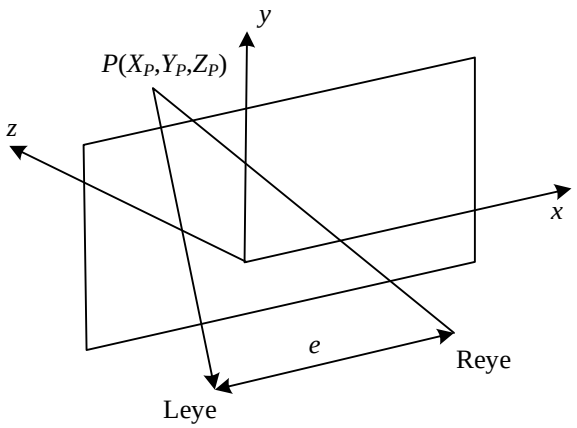

Figure 2. Double center projection

The left viewpoint Leye and the right viewpoint Reye are located on axis X, the distance between the two viewpoints is e, and the center of the line connecting the two viewpoints is the origin of the coordinates, then the coordinates of the left viewpoint are $(-\mathrm{e}/2,0,0)$, and the coordinates of the right viewpoint are $(+\mathrm{e}/2,0,0)$. The plane of projection is parallel to the XY-plane, and the distances to the right and left viewpoints are d. The coordinate of a point $P(xp,yp,zp)$ in three-dimensional space in the projection of the left viewpoint is (x_1,y_1,z_1), and the coordinate of the projection of the right viewpoint is (x_r,y_r,z_r), so that the coordinates of the point $zl=zr=d$. The parametric equations of the projected lines of the point $P(x_p,y_p,z_p)$ and Reye are the parametric equation of the Reye projection line is:

$$\begin{aligned} x &= x_p + t(e/2 - x_p) \\ y &= y_p + t(0 - y_p) \\ z &= z_p + t(0 - z_p) \end{aligned} \tag{1}$$

$\mathrm{z}=d$ in the plane of projection can be obtained:

$$t = \frac{z_p - d}{z_p} \tag{2}$$

Bringing Eq. (2) into Eq. (1) yields the coordinates of point P in the plane of projection (x_r,y_r):

$$x_r = \frac{(x_p - e/2)d}{z_p} + \frac{e}{2}, y_r = \frac{y_p d}{z_p} \tag{3}$$

Similarly, the coordinates of the projected points of point P and Leye's projected line on the projective plane are:

$$x_l = \frac{\left(x_p + e/2\right)d}{z_p} - \frac{e}{2}, y_l = \frac{y_p d}{z_p} \tag{4}$$

Horizontal parallax can be obtained:

$$E = \left(x_r - x_l\right) = -\frac{ed}{z_p} + e \tag{5}$$

It follows that when $z_p > d$, $0 < E < e$, this is positive parallax. When $z_p < d$, $E < 0$, this is negative parallax. And when $z_p = d$, $E = 0$, this is zero parallax. Using the dual-center projection algorithm, the left and right eye images of the object in three-dimensional space can be obtained by setting the dual viewpoints, so as to generate stereo image pairs.

2.2 Multi-channel stereoscopic display

In order to make the large-scale ring screen display system show realistic and smooth scene images so that users can experience immersive immersion through specific interaction methods, the system can generate high-quality scene images in real-time. The following is an in-depth study of the four key technologies of the multi-channel ring screen display system: nonlinear distortion correction, digital image edge fusion and seamless splicing, data synchronization, and inter-channel color and luminance balance [24-25].

Geometric distortion correction technology is one of the key technologies in virtual reality projection systems. The reason why the multi-channel large screen display system should carry out the nonlinear distortion correction of the image is mainly due to the fact that when the projector is not projected onto the screen or projected onto a non-planar screen, the geometric shape of the image is deformed, resulting in geometric distortion, i.e., what is usually referred to as trapezoidal distortion and nonlinear distortion.

The overall steps of the software nonlinear distortion correction algorithm used are as follows, Figure 3 for the nonlinear distortion correction process.

1) Determine the proposed projection plane to be projected on the projector and find out the coordinate correspondence of the points between this plane and the projection surface.

2) Determine the projection surface function of the projection screen relative to the projector in the polar coordinate system.

3) According to the correspondence in step 2, the texture is mapped onto the surface of the projection screen by cyclic texture mapping, and the deformation correction of the image is realized after mapping.

4) Before the nonlinear distortion correction, copy the real-time generated image of each channel from the frame buffer, use it as the texture pattern, and mesh the texture according to the principle of equirectangular division.

5) Carry out channel splicing, raster alignment, and digital image edge fusion and seamless splicing between channels so that the multi-channel display a complete and seamless picture of the wide-view scene, thus completing all the nonlinear distortion correction process.

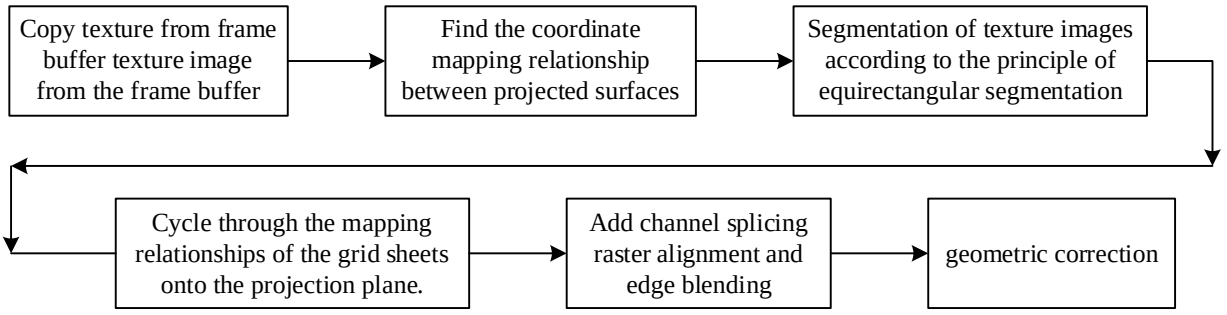

Figure 3. Nonlinear distortion correction process

Fig. 4 shows the general diagram of the curved-column surface projection system. Figure 5 shows the schematic for texture mapping. Shown is a normal cylindrical projection system with orthographic projection, where the projector is located at the point. AMB is the projection screen and is the orthographic projection plane.

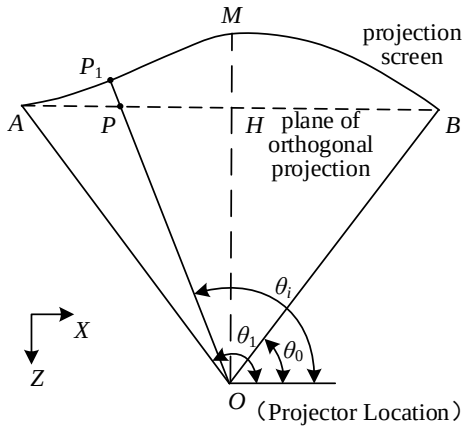

Figure 4. General diagram of the projection system of the cylinder

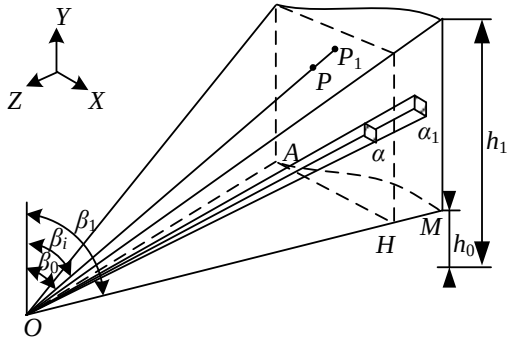

Figure 5. Texture mapping diagram

An image projected from O point onto AMB will produce a nonlinear deformation. To correct the deformed image, the mapping relationship between the plane AHB and the projection plane in two dimensions has to be established, so it is first necessary to find the mapping relationship between the

points on the projection plane and the points on the orthographic projection plane P only. Let the equation of the spatial polar coordinate system of AMB be:

$$\begin{aligned} r &= f(\theta), (\theta_0 \le \theta \le \theta_1) \\ h_0 &\le y \le h_1 \end{aligned} \tag{6}$$

Where θ_0, θ_1 is the angle of the boundary between the ends of the projection screen, h_0, h_1 are the height values of the ends of the projection screen. If θ_1, β_i are known, then:

$$\begin{aligned} p_{1x} &= f(\theta_i) * \cos(\theta_i) \\ p_{1z} &= f(\theta_i) * \sin(\theta_i) \\ p_{1y} &= f(\theta_i) / \tan(\beta_i) \end{aligned} \tag{7}$$

From the above analysis, it can be seen that the mapping relationship between face AHB and face AMB can be found if the mesh is divided on face AHB so that the value of θ_i, β_i at each mesh intersection is known. Mesh partitioning algorithms include orthogonal partitioning, primary polynomial piecewise correction algorithms, and so on. To enable θ_i, β_i to be determined, this paper proposes a new angular equidistant meshing algorithm, whose basic idea is to make the angle between each row and column of the mesh and the projector position the same. The purpose of meshing is to linearize the nonlinear deformation within each gridlet and to make the θ_i, β_i value of each grid intersection knowable. Then the coordinates of the grid points in rows i and J of the texture are:

$$\begin{aligned} p_x &= (\operatorname{ctg}\theta_1 - \operatorname{ctg}\theta_1) / (\operatorname{ctg}\theta_0 - \operatorname{ctg}\theta_1) \\ p_y &= (\operatorname{ctg}\beta_i - \operatorname{ctg}\beta_1) / \operatorname{ctg}\beta_0 - \operatorname{ctg}\beta_1) \end{aligned} \tag{8}$$

When the position of the projector or screen changes, i.e. the projector position is not orthographic, the above method can still be applied by changing the values of θ_i and β_i accordingly. This correction method is applicable to general quadratic surfaces such as cylindrical, parabolic, spherical, hyperbolic surfaces, and some typical polar parametric surfaces such as bath line cylindrical surfaces and helical cylindrical surfaces. Spherical projection systems can also use this method to achieve nonlinear distortion correction, and the case of spherical surfaces will be specifically analyzed later.

3 Virtual Reality-based Landscape Design Lighting Analysis

3.1 Illumination

Illuminance, luminous intensity, luminous flux and brightness are the basic photometric units in common use. Their concepts are as follows.

1) Illuminance is the density of luminous flux per square meter of area in a unit of time, expressed by the symbol E. Let the luminous flux on the surface of the unit at any point on the surface element is $d\phi$, the area of the surface element is dA, then:

$$E = \frac{d\phi}{dA} \tag{9}$$

Lux is the unit of luminous intensity, expressed by the symbol $1\mathrm{x}$.

2) Luminous intensity is any point of light source in any direction in the stereoscopic angle element of the luminous flux emitted within the stereoscopic angle element and the quotient of the stereoscopic angle element, known as the luminous intensity, expressed by the symbol I, the unit of candelas, expressed by the symbol cd:

$$I = \frac{d\phi}{d\Omega} \tag{10}$$

3) Luminous flux usually refers to the energy of light radiation (or radiant power) perceived by the human eye. The symbol is Φ, the unit is lumen, and it is represented by the symbol $1\mathrm{m}$:

$$\phi = K_m \int \phi_{e,\lambda} V(\lambda) d(\lambda) \tag{11}$$

Where $\phi_{e,\lambda}$ is the monochromatic radiant energy flux at a wavelength of λ (W), $V(\lambda)$ refers to the visual spectral photovoltaic efficiency of a CIE standard photometric observer, and K_m is the maximum spectral photovoltaic efficacy $(1\mathrm{m/W})$ which was K_m positioned by the International Committee of Weights and Measures in 1976 $6831\mathrm{m/W}$.

4) Brightness is the density of light intensity on the surface of a unit in any direction. It is represented by the symbol L and the unit is $\mathrm{cd/m^2}$:

$$L_\theta = \frac{dI_\theta}{dA \cdot \cos\theta} \tag{12}$$

Since the luminosity is different in each direction, it is necessary to indicate the direction for the luminosity.

3.2 Distribution of Landscaping Brightness

Professor Kittler proposed a mathematical model of the clear sky brightness distribution based on his analysis of decades of observational data [26], which was later established as the CIE standard clear sky brightness distribution function:

$$L_P = L_Z \left\{ \frac{\left[0.91 + 10\exp(-3\delta) + 0.45\cos^2\delta\right][1 - \exp(-0.32/\cos\varepsilon)]}{\left[0.91 + 10\exp\left(-3Z_0\right) + 0.45\cos^2 Z_0\right][1 - \exp(-0.32)]} \right\} \tag{13}$$

Where, L_P is the brightness of the sky P points $\left(\mathrm{cd/m^2}\right)$, L_Z is the zenith brightness $\left(\mathrm{cd/m^2}\right)$, ε is the angle between P points and the zenith, Z_0 is the zenith angle of the sun, δ is the angle between the sky P points and the sun, Fig. 6 shows a schematic diagram of the three-dimensional angle of the sky. The sun's light shines from the southeast, northwest, and zenith directions, respectively to formulate the object, forming certain angles, thus creating different angles of light.

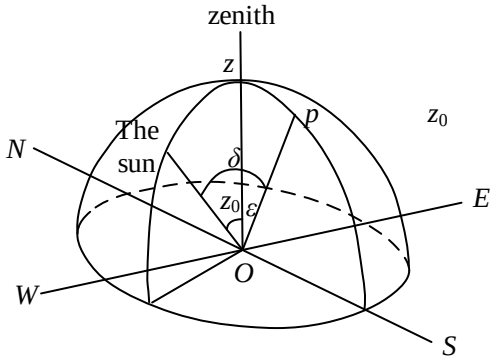

Figure 6. Sky cube diagram

The brightness of the fully cloudy sky is equal in different directions at the same altitude, but from the horizon to the zenith, its brightness is not the same at different altitudes, and its brightness change expression is:

$$L_\theta = L_Z\left(\frac{1+2\sin\theta}{3}\right) \tag{14}$$

where L_θ refers to the brightness of the sky at an angle to the ground θ and L_Z is the zenith brightness $\left(\theta = 90^\circ\right)\left(\mathrm{cd}/\mathrm{m}^2\right)$.

3.3 Lighting coefficient

Lighting is the work of introducing natural light into the room to make the room bright. The lighting coefficient is used as an evaluation index of lighting effect in lighting design [27-28]. Generally, indoor light mainly comes from direct sunlight, reflected light from the sky and reflected light from the room, so the expression of the daylighting coefficient at any point in the room is as follows:

$$C = C_t + C_{wf} + C_{nf} \tag{15}$$

Figure 7 shows the composition of natural light in the room. C is the lighting coefficient at any point in the room, $\mathrm{C_t}$ is the component of direct sunlight for C, $\mathrm{C_{wf}}$ is the component of reflected light from the sky for C, and $\mathrm{C_{nf}}$ is the component of reflected light from the room for C.

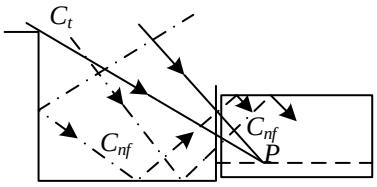

Figure 7. Indoor natural light composition

The expression for the component $\mathrm{C_t}$ of direct sunlight for lighting factor C is given below:

$$C_t = \frac{E_n}{E_w} \times 100\% \tag{16}$$

where E_n is the illuminance $(1x)$ at any point in the room, and E_w is the outdoor illuminance $(1x)$ at the same time as E_n, without shading. C_{wf} and C_{nf} are also defined following equation (16).

3.4 Lighting calculations

Lighting methods are used to determine the basis of the design of lighting outlets and lighting analysis; generally speaking, the common methods are top lighting, side lighting and mixed lighting [29-30]. As long as the top lighting coefficient and the side lighting coefficient are calculated, the mixed lighting coefficient can often be obtained by analyzing and calculating.

Top lighting has:

$$\bar{C} = C_d K_\tau K_\rho K_g (\%) \tag{17}$$

Side lighting is available:

$$C_{\min} = C_d' K_\tau K_\rho' K_w K_c (\%) \tag{18}$$

Where, C_d for the skylight lighting coefficient, C_d' for the side window lighting coefficient, K_ρ for the top lighting indoor reflection incremental coefficient, K_ρ' for the side lighting indoor reflection incremental coefficient, K_g for the height to span ratio correction coefficient, K_w for the side of the outdoor building light-blocking discount coefficient for side-lighting, K_c for the side of the side of the light window width correction coefficient, $K_c = \frac{\sum b_c}{L}$, where $\sum b_c$ is the length of the building in the direction of the total of the width of the windows of any wall, L is the length of the building, K_τ for the total transmittance coefficient, then $K_\tau = \tau \tau_c \tau_w \tau_j$, where τ is the transmittance coefficient of the lighting material, τ_c is the window construction light-blocking discount factor, τ_w is the window glass pollution discount factor, τ_j is the indoor structure light-blocking discount factor.

4 Analysis of the effectiveness of virtual reality integration landscape design

4.1 Analysis of subjective evaluation of virtual scenes

In order to study the effect of virtual reality integration landscape design, this paper scores the subjectivity of the two environments by 15 women and 15 men, and the data were subjected to a double overall independent samples t-test, the subjects were grouped by gender, the correlation between subjective scores and gender were analyzed, and there was no statistically significant difference in the subjective evaluation of the environments by different genders.

The subjective questionnaire results were counted to analyze the scoring of different scenes. Table 1 displays the subjective assessment of the virtual scenes. The Sig value of environmental suitability of

the two spatial designs is 0.037, which is less than 0.05, indicating that there is a significant difference between the suitability of the two environmental designs. The significance level between environmental satisfaction and satisfaction with life is 0.909, which is a significant difference. The difference in spatial permeability between the two designs is -5.926, which implies that the landscape design that incorporates virtual technology has a stronger spatial permeability. In terms of mood, the difference between the two was the largest, with the virtual technology spatial design being 7.945 more than the normal design, a significant difference that indicates a huge advantage for the virtual technology spatial design. In terms of attention, subjects reported that it was easier to concentrate in the virtual design space, with a difference of -5.241 and a Sig value of 0.014 between the two.

Table 1. Virtual scene subjective evaluation

	Adapt	Satisfact	Emotion	Attention	Color	Space scale	Thorough	All
Cons	0.664	0.909	0.639	0.846	0.560	0.730	0.579	0.632
Sig	0.037	0.040	0.068	0.014	0.095	0.049	0.034	0.041
Difference value	-5.073	-5.615	-7.945	-5.241	-5.890	-2.373	-5.926	-2.606
95% of the location letter interval	0.349	0.781	0.237	0.233	0.542	0.406	0.946	0.774

Therefore, there is a large difference between the subjective feelings about the space expressed by the subjects in the two scenarios, real and virtual, and it can be assumed that the subjective feelings of the subjects in the virtual environment are more effective than the ordinary environment design.

4.2 Analysis of Environmental Human Perception and Attentional Differences

After that, the efficiency of the subjects in the two environments is analyzed. Two environmental experimental scenarios were selected for experimentation, two for each scenario, S1 and S2 for virtual landscape design scenarios, and S3 and S4 for traditional landscape design scenarios, respectively, to study the subjects' attention in two different scenarios, and this paper mainly reflects the subjects' attention through the accuracy of the questions. The accuracy of the questions is what mainly reflects the subjects' attention in this paper. Because the questions are set with a certain degree of difficulty, it is very much a test of the subjects' mental concentration and state of mind. Figure 8 shows the subjective questionnaire QC (X-Bar) R Chat, Figure 8(a) is the -Subgroup mean plot, and Figure 8(b) is the R Chat plot. After the data statistics, the average correct answer rate of 30 subjects was 88.43%. The analysis of subjects' subjective questionnaires by QC (X-Bar) R Chat shows that the upper confidence limit of Mean UCL mean is 0.9508, the lower confidence limit of Mean LCL mean is 0.6179, the mean of Range CLR is 0.9152, and the upper confidence limit of Range UCL R is 0.6435. It shows that all 4 experimental scenarios can keep the subjects' correct rate high, but the deviation of R is large, and the individualization of the subjects is significant. Therefore, it is meaningful to statistically compare the correct rates of all subjects completing the task under different scenarios and to analyze the differences in each subject's attention in different scenarios one by one, which is also meaningful for analyzing individualized preferences.

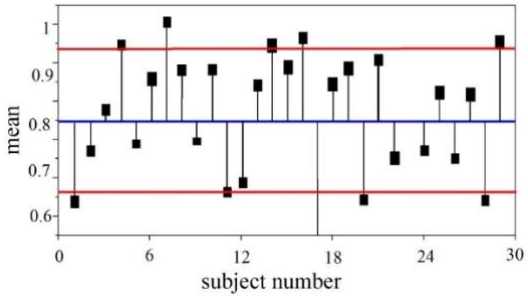

(a) Subgroup mean

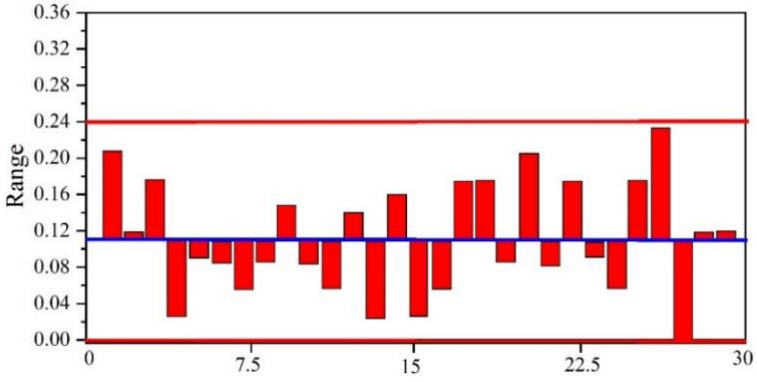

(b) R Chat

Figure 8. Subjects were subject to subjective questionnaire qc (x-bar) rchat

Then the statistics of the 30 subjects' correct rates in the task completion phase for the four experimental scenarios were conducted. The statistical analysis of the box-and-line plot of the correct rates of the experimental scenarios is shown in Figure 9. From the figure, it can be seen that the mean of the correct rate under the four scenarios is ordered as A > B > D > C, the median is ordered as A > B > D > C, and the range of variation of B is the smallest, and the correct rate is the most stable. The mean value of the correct rate in the virtual design scenario in S1 was 91%, and the subjects in the virtual design scenario in S2 had a 90% correct rate in task completion. In contrast, the correct rate in the traditional design scenario in S3 was 10% less than in S1 and 9% less than in S2. The mean value of answer accuracy in the traditional design scenario in S4 was also around 80%, which was approximately the same as in the S3 scenario. This figure proves that environmental differences can affect the attention levels of subjects in different scenarios. Compared to the normal scenario design, people in the virtual design scenario had a 7%-10% increase in attention level.

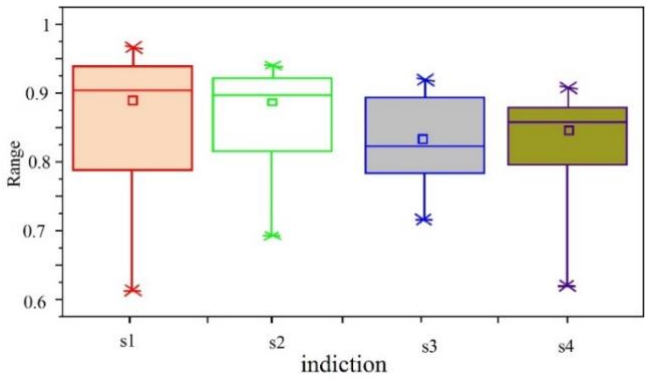

Figure 9. Statistical analysis of the accuracy box diagram of the experiment scene

4.3 EEG Signal Analysis

In order to study the differences in brain arousal levels between different landscape designs, this paper analyzes the brain arousal levels of the two environments by collecting the EEG signals induced by the traditional landscape design and the virtual landscape design from the subjects at the five frequencies of 8 Hz, 9 Hz, 10 Hz, 11 Hz, and 12 Hz, and obtaining the accuracy by using the CCA algorithm for real-time online processing. In this paper, six electrode points P1, Pz, P2, O1, Oz, and O2 in the visual area, i.e., occipital area, were selected for analysis and processing to compare the

arousal level of the brain under the two stimulation modes, so as to evaluate the effect of landscape design. Figure 10 shows the comparison of brain arousal levels in two stimulation modes.

The frequency and stimulation mode were used to determine the average value in this paper. Among them, there is a significant difference in the accuracy of the two environmental stimulation sources under the frequencies of 8Hz, 9Hz, 10Hz, 11Hz, and 12Hz. At 8Hz, the stimulation level of traditional landscaping was 78%, while the brain stimulation level of virtual reality-based landscaping was 84%. At 11Hz, the arousal level of the brain was 72% for traditional landscaping and 10% more for virtual landscaping than for traditional landscaping. Overall, the average level of brain frequency induced by virtual landscape design is 8%-10% higher than that of traditional landscape design, and there is a big difference between the brain arousal levels of the two stimulation modes. It can be assumed that the virtual landscape design stimulation source induces the EEG signals better than that of traditional landscape design.

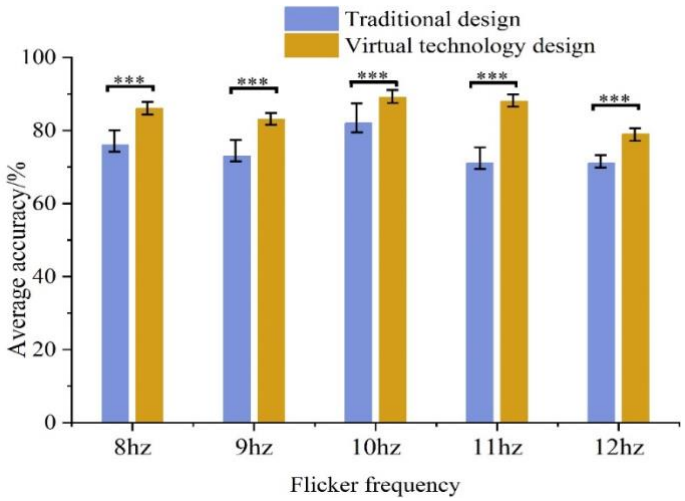

Figure 10. Shows a comparison of arousal levels in the brain

5 Conclusion

This paper studies the integration effect of virtual reality technology and landscape design and analyzes the advantages and disadvantages of the two design methods by comparing the effects of traditional landscape design and virtual reality landscape design. These conclusions are drawn:

The Sig value of the environmental adaptability of the two spatial designs is 0.037, which is less than 0.05, indicating that there is a significant difference between the applicability of the two environmental designs, and the subjective scores indicate that the landscape design of virtual reality technology is better than the traditional design method.

The mean value of the correctness rate was 91% in the virtual design scenario in S1, 81% in the traditional design scenario in S3, and 84% in the traditional design scenario in S4, and people's attention was improved by 7%-10% in the virtual design scenario compared to the ordinary scenario design.

The average level of brain frequencies induced by virtual landscape design was 8%-10% higher than that of traditional landscape design, and the effect of EEG signals induced by virtual landscape design stimulus sources was better than that of traditional landscape design.

Funding:

This research was supported by the Sichuan Social Practice First-class Course: Artistic Lighting Landscape Design Training Topic (YLKC01933).

References

[1] Shan, P., & Sun, W. (2021). Research on landscape design system based on 3d virtual reality and image processing technology. Ecological Informatics(9), 101287.

[2] Jin, Y., Chen, Y., & Qu, J. (2022). Interior soft decoration product design based on 3d modeling and image processing technology. Mobile Information Systems.

[3] Tian, F. (2021). Immersive 5g virtual reality visualization display system based on big-data digital city technology. Mathematical Problems in Engineering, 2021(3), 1-9.

[4] Zhang, X., Fan, W., & Guo, X. (2022). Urban landscape design based on data fusion and computer virtual reality technology. Wireless Communications and Mobile Computing, 2022(9).

[5] Winkler, I. (2023). Towards sustainable virtual reality: gathering design guidelines for intuitive authoring tools. Sustainability, 15.

[6] Zhang, G., & Kou, X. (2021). Research and application of new media urban landscape design method based on 5g virtual reality. Journal of Intelligent and Fuzzy Systems(1), 1-9.

[7] Gang, J., & Li, Y. (2021). Simulation design and implementation of voice landscape quantification in virtual reality based on cloud computing. Mobile Information Systems.

[8] Zhang, Y. (2021). Application of intelligent virtual reality technology in college art creation and design teaching. Journal of Internet Technology(6), 22.

[9] Zhang, X., Yan, S., & QuanQi. (2021). Virtual reality design and realization of interactive garden landscape. Complexity, 2021.

[10] Wenhao, D., & Shi, G. (2021). Multisensor information fusion-assisted intelligent art design under wireless virtual reality environment. Journal of Sensors(Pt.11), 2021.

[11] Cai, K., Huang, W., & Lin, G. (2022). Bridging landscape preference and landscape design: a study on the preference and optimal combination of landscape elements based on conjoint analysis. Urban Forestry & Urban Greening.

[12] Huang, C. M., Liao, J. Y., Lin, T. Y., Hsu, H. P., & Guo, J. L. (2021). Effects of user experiences on continuance intention of using immersive three-dimensional virtual reality among institutionalized older adults. Journal of Advanced Nursing(2).

[13] Kong Y.Research on the Application of Environmental Art Design Based on the Combination of VR and Panoramic Video Technology[J].Scientific programming, 2021(Pt.11):2021.

[14] Zhou, Q. (2020). Research on architectural space design of coastal cities based on virtual reality technology. Journal of Coastal Research, 115(sp1), 13.

[15] Ling, H. (2019). Design of visual 3d scene based on virtual reality technology. Basic & clinical pharmacology & toxicology.(S1), 125.

[16] Lu, G., Xue, G., & Chen, Z. (2011). Design and Implementation of Virtual Interactive Scene Based on Unity 3D. International Conference on Advanced Design and Manufacturing Engineering.

[17] Zeng, L., & Dong, X. (2021). Artistic style conversion based on 5g virtual reality and virtual reality visual space. Mobile Information Systems.

[18] Wang, H. (2019). Landscape design of coastal area based on virtual reality technology and intelligent algorithm. Journal of Intelligent and Fuzzy Systems(5).

[19] Basu, T., Bannova, O., & Camba, J. D. (2021). Mixed reality architecture in space habitats. Acta Astronautica, 178(152), 548-555.

[20] Jing, W. (2015). Study on application of virtual reality technique in environmental artistic design. International Journal of Technology, Management(010), 000.

[21] Kim, S., Kim, J., & Kim, B. (2020). Immersive virtual reality-aided conjoint analysis of urban square preference by living environment. Sustainability, 12.

[22] Maolin, G., Wangyong, L., & Lu, F. U. (2016). Spatial statistical analysis on pm_(2.5) in chengdu based on improved moran's i. Environmental Science & Technology.

[23] Lyu, K., Brambilla, A., Globa, A., & Dear, R. D. (2023). An immersive multisensory virtual reality approach to the study of human-built environment interactions. Automation in construction.

[24] Li, L., Zhu, W., & Hu, H. (2021). Multivisual animation character 3d model design method based on vr technology. Complexity, 2021(4), 1-12.

[25] Gao, G., & Li, W. (2021). Architecture of visual design creation system based on 5g virtual reality. International Journal of Communication Systems(4).

[26] David C. Schwebel, Joan Severson, & Yefei He. (2017). Using smartphone technology to deliver a virtual pedestrian environment: usability and validation. Virtual Reality.

[27] Surer, E., Erkayaoglu, M., Ozturk, Z. N., Yucel, F., Biyik, E. A., & Altan, B., et al. (2021). Developing a scenario-based video game generation framework for computer and virtual reality environments: a comparative usability study. Journal on multimodal user interfaces(4), 15.

[28] Seth, A., & Oliver, V. J. H. (2011). Virtual reality for assembly methods prototyping: a review. Virtual Reality.

[29] Jo, D. S., Yang, U. Y. Y., & Son, W. H. (2008). Design evaluation system with visualization and interaction of mobile devices based on virtual reality prototypes. Etri Journal, 30(6), 757-764.

[30] Guo, Z., Zhou, D., Zhou, Q., Mei, S., Zeng, S., & Yu, D., et al. (2020). A hybrid method for evaluation of maintainability towards a design process using virtual reality. Computers & Industrial Engineering, 140(Feb.), 106227.1-106227.14.